Evidence for superdeformed shape isomeric states in ^{28}Si at excitations above 40 MeV through observations of selective particle decays of $^{16}O+^{12}C$ resonances in ^{8}Be and alpha channels

M. A. Eswaran, Suresh Kumar, E. T. Mirgule, D. R. Chakrabarty, V. M. Datar, N. L. Ragoowansi, and U. K. Pal
Nuclear Physics Division, Bhabha Atomic Research Centre, Bombay 400 085, India
(Received 23 December 1991)

Excitation functions of the reactions $^{12}C(^{16}O,^{8}Be)^{20}Ne$ and $^{12}C(^{16}O,^{4}He)^{24}Mg$ leading to several states have been measured in the range $E_{c.m.}=25.7$–38.6 MeV. From cross channel correlation analysis two intermediate resonance structures at $E_{c.m.}=26.9$ and 29.5 MeV corresponding to excitation energies of 43.7 and 46.2 MeV in ^{28}Si have been identified. Angular distribution measurements for $^{12}C(^{16}O,^{4}He)^{24}Mg_{g.s.}$ have also been made at the lower resonance at $E_{c.m.}=26.9$ MeV which enable spin assignment of $J^{\pi}=14^{+}$ to this resonance. Striking observation of preferential ^{8}Be decay of both the resonances to the 8-particle–4-hole states in ^{20}Ne is interpreted as evidence for the resonances to be highly deformed shape isomeric configurations in ^{28}Si expected from deformed shell-model calculations.

PACS number(s): 25.70.Ef, 25.70.Gh

I. INTRODUCTION

In spite of extensive experimental and theoretical efforts, a comprehensive understanding of nature of the heavy-ion resonances observed in collisions involving any two of the nuclei ^{12}C, ^{16}O, ^{24}Mg, ^{28}Si, etc. is still lacking [1,2]. There have been explanations of such heavy-ion resonances in terms of dynamical models [3–5] in which these resonances are viewed as being a consequence of both weak absorption and the existence of pockets in the interaction potential of two ions. There are also explanations in terms of compound nucleus models [6–8] in which shell stabilization of highly deformed compound nuclei may result in shape isomeric states with large overlap with heavy-ion decay channels.

It has been particularly suggested that the resonances might be manifestations of shape isomeric states of a compound system produced in the superdeformed second well in the potential-energy surfaces akin to fissioning shape isomers in the actinide region [9]. Specific evidence of this explanation to be applicable has been found in the case of the compound system ^{24}Mg observed in the resonances of $^{12}C+^{12}C$ ions [10] and also in the case of ^{56}Ni observed in the resonance structures of the $^{28}Si+^{28}Si$ system [11].

In the present paper we report on the experimental observations which provide evidence for such a shape isomeric nature of the two resonances in the $^{16}O+^{12}C$ system leading to excitation energies above 40 MeV in ^{28}Si. Specifically, simultaneous measurements of excitation functions for the reactions $^{12}C(^{16}O,^{8}Be)^{20}Ne$ and $^{12}C(^{16}O,\alpha)^{24}Mg$ leading to several discrete states of ^{20}Ne and ^{24}Mg were made in the energy range $E_{c.m.}=25.7$–38.6 MeV. Particularly in the ^{8}Be channel, the excitation functions leading to 8-particle–4-hole states of ^{20}Ne are being reported for the first time. These measurements are the ones which provide evidence for the $^{16}O+^{12}C$ resonances to be of the nature of shape isomeric states of the compound system. Angular distribution measurements leading to spin assignments of one of the resonances are also being reported in this work. Preliminary results of this work have been reported earlier [12].

II. EXPERIMENTAL PROCEDURE

The excitation functions for the reactions $^{12}C(^{16}O,^{8}Be)^{20}Ne$ and $^{12}C(^{16}O,\alpha)^{24}Mg$ were measured with a momentum-analyzed beam of $^{16}O(5^{+})$ from the Bhabha Atomic Research Centre—Tata Institute of Fundamental Research (BARC-TIFR) 14UD Pelletron at Bombay in the beam energy range of 60–90 MeV in steps of 1 MeV. The overall uncertainty in the incident energy of the beam is estimated to be less than ± 30 keV.

Three surface-barrier detector telescopes were set at 6°, 9°, and 16°, respectively, to the beam for the particle identification of the reaction products in the scattering chamber of 1 m diam. The telescope set at 9° was of 11 mm diam at a distance of 13.3 cm from the target subtending a solid angle of 5.37 msr with angular acceptance of $\pm 2.36°$ at the target. The depletion layer thicknesses of ΔE and E detectors were 30 μm and 2 mm, respectively. The relatively larger solid angle of this detector was chosen such that it enabled detection of ^{8}Be, the ground state of which decays into two alpha particles moving in a narrow forward cone. The ground state of ^{8}Be is 92 keV unbound for decay into two alpha particles and detection of both the alpha particles simultaneously in the detector is required for identification of ^{8}Be [13]. The actual effective solid angle for ^{8}Be (ground-state) detection was calculated numerically with a computer program [14] and it was in the range of 10–20 % of the geometric solid angle for the energies of ^{8}Be in the present work. The efficiency for simultaneous detection of two alpha particles arising from the decay of excited states of ^{8}Be is negligible. This telescope enabled detection of alpha particles as well as ^{8}Be for simultaneous measurements of excitation functions for the reactions $^{12}C(^{16}O,\alpha)^{24}Mg$ and $^{12}C(^{16}O,\ ^{8}Be_{g.s.})^{20}Ne$.

The telescopes set at 6° and 16° were of depletion layer

thicknesses 40 μm and 2 mm for ΔE and E detectors, respectively. They were at a distance of 25.5 cm from the target subtending solid angle of 0.43 msr with angular acceptance of $\pm 0.45°$. These were suitable for identification of alpha particles for excitation function measurements of the reaction ^{12}C (^{16}O ,α)^{24}Mg.

The beam was collimated to a 2.5 mm spot on the target by tantalum collimators. The target was a natural carbon foil of thickness 104 $\mu g/cm^2$ for excitation function measurements. The target thickness was estimated by measuring the energy loss of 5.486 MeV alpha particles passing through it. The beam was stopped in a Faraday cup in which accumulated charge was measured in a current integrator and used as the monitor in the excitation function measurements.

The ΔE-E two-dimensional spectra, recorded in an on-line computer for all the telescopes enabled the setting up of flexible two-dimensional gates for particle identification and thereby building one-dimensional energy spectra corresponding to different particles. In the case of the 9° telescope in the ΔE-E two-dimensional spectra, ^{8}Be can be simulated by ^{7}Li [15]. However, since the Q values of the reaction $^{12}C(^{16}O,^7Li)$ is 14.8 MeV more negative than the $^{12}C(^{16}O,^8Be)$ reaction, this does not pose any problems in identifying the ^{8}Be groups of higher energies.

In the case of angular distribution measurements for the reaction $^{12}C(^{16}O,\alpha)^{24}Mg_{g.s.}$ a carbon foil of thickness 50 $\mu g/cm^2$ was used. Six surface-barrier detectors of 2 mm thickness were used for detection of alpha particles and these were set 10° apart at distances of 17.9–20.5 cm from the target subtending solid angles of 0.76–1.5 msr with an angular acceptance of about $\pm 0.7°$. With the alpha group leading to $^{24}Mg_{g.s.}$ as the highest-energy particle group, there was no difficulty in identifying this group in the surface-barrier detector spectra for angular distribution measurements. A surface-barrier detector of 300 μm thickness was mounted at a fixed forward angle to the beam and the elastically scattered peak from the target in this detector was used as a monitor for the angular distribution measurements to normalize the data. The angular distribution measurements were taken in steps of 1.6°–2.5° with an overlapping point available between the adjacent detectors to enable normalization among different detectors. Accuracy of angular positioning of the detection in the scattering chamber was checked to be better than 0.1°. The measurements covered the angular range of 6°–77° in the laboratory corresponding to 8.5°–101.3° in the center-of-mass system.

III. EXPERIMENTAL MEASUREMENTS

A. Excitation functions for $^{12}C(^{16}O, ^8Be)^{20}Ne$ and $^{12}C(^{16}O,\alpha)^{24}Mg$ reactions

An example of the ^{8}Be spectrum detected in the surface-barrier detector telescope at 9° and recorded in the computer by an appropriate two-dimensional gate on the ΔE-E plot as described in the previous section, at a beam energy of 63 MeV is shown in Fig. 1(a). The ^{8}Be groups leading to $^{20}Ne_{g.s.}$, 1.63 MeV 2^+, 4.25 MeV 4^+ in

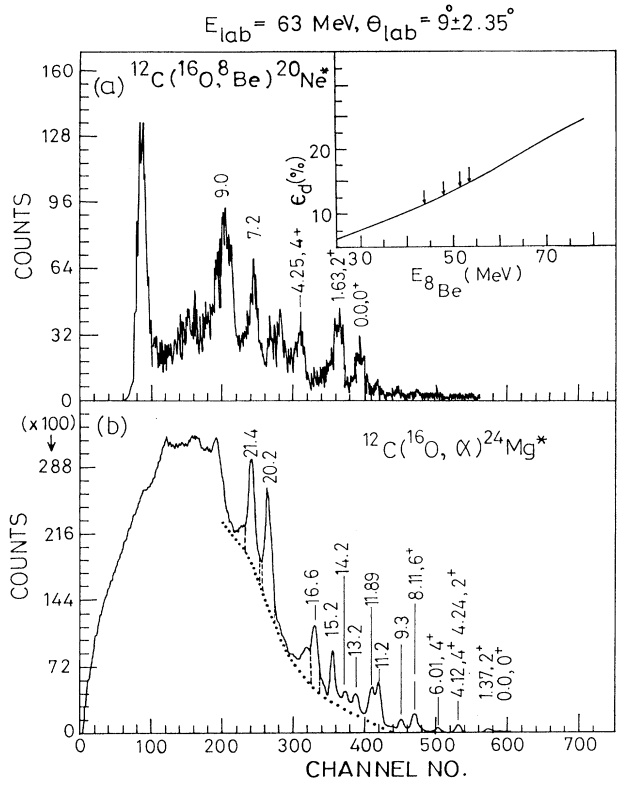

FIG. 1. (a) The ^{8}Be spectrum recorded in the ΔE-E detector telescope from the reaction $^{12}C(^{16}O,^8Be)^{20}Ne$ at $E(^{16}O)=63$ MeV. The numbers above the peaks denote the excitation energies in MeV of states in ^{20}Ne. The inset shows the detection efficiency ϵ_d of the ^{8}Be detector, as a function of energy of ^{8}Be and the arrows indicate the energies corresponding to the marked peaks in the spectrum. (b) The alpha spectrum recorded in the same telescope from the reaction $^{12}C(^{16}O,\alpha)^{24}Mg$. The dotted line indicates the smooth continuum which was subtracted for evaluation of excitation function measurements.

the reaction $^{12}C(^{16}O, ^8Be)^{20}Ne$ are clearly identified. The ^{8}Be groups corresponding to 7.2 and 9 MeV excitation in ^{20}Ne are also marked in the figure. For the excitation functions the counts in these five peaks were evaluated respectively for the bombarding energy range 60–90 MeV and these are shown in Fig. 2.

In the same telescope at 9°, the alpha spectrum recorded in the computer by an appropriate two-dimensional gate on the ΔE-E plot is also shown in Fig. 1(b). The alpha groups leading to various states of ^{24}Mg in the reaction $^{12}C(^{16}O,\alpha)^{24}Mg$ can be clearly identified. Above the 10 MeV excitation in ^{24}Mg, the alpha particle peaks are riding on a continuum which increases significantly at higher excitations. In addition to the alpha particles from the reaction $^{12}C(^{16}O,\alpha)^{24}Mg$, continuum can arise in other reactions such as the breakup of projectile or target or the excited residual nuclei. However, the alpha particle groups feeding excited states up to 21.4 MeV in ^{24}Mg can be identified from the kinematically expected energies. The overall energy resolution of the particle peak is about 550 keV. For the excitation functions, a smooth continuum below the peaks were subtracted and for 19

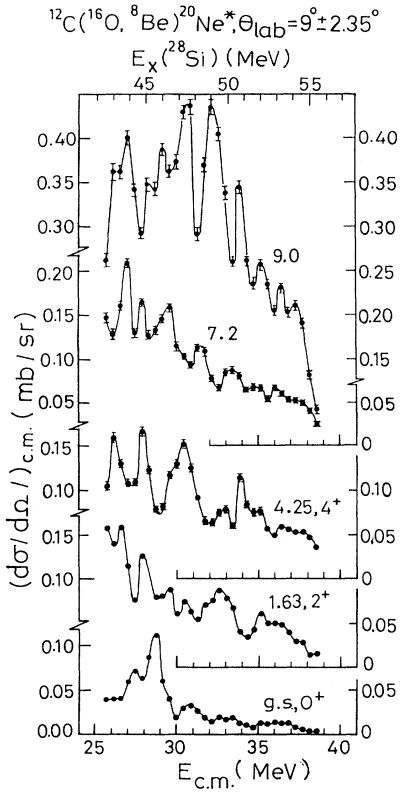

FIG. 2. Excitation functions for the reaction $^{12}C(^{16}O,^{8}Be)^{20}Ne$ at $\Theta_{lab}=9°$ to different states of ^{20}Ne. The excitation energies of the state of ^{20}Ne are shown in MeV.

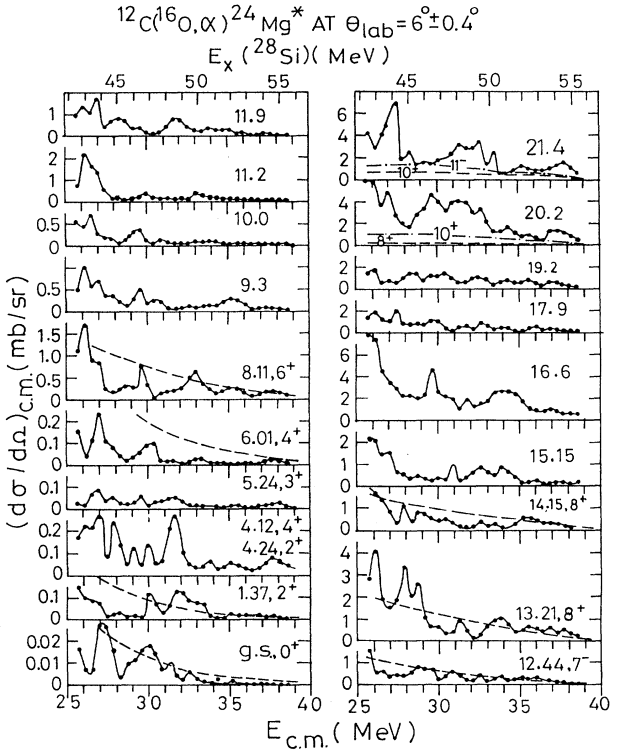

FIG. 3. Excitation functions for the reaction $^{12}C(^{16}O,\alpha)^{24}Mg$ at $\Theta_{lab}=6°$ to various states of ^{24}Mg, the energies of which are shown in MeV. The dashed lines show the statistical-model calculations of the average cross sections. These are shown only for those states which are judged to be single states from the widths of the peaks in the spectrum.

peaks the excitation functions could be determined for the bombarding energy range 60–90 MeV and these are shown in Figs. 3, 4, and 5 corresponding to telescopes at 6°, 9°, and 16°, respectively. Of the 19 peaks for which excitation functions were obtained, some of them are for single states in ^{24}Mg and some of them are due to unresolved adjacent states as judged from the widths of the peaks.

B. Angular distributions for $^{12}C(^{16}O,\alpha)^{24}Mg_{g.s.}$

The angular distribution data were measured for the reaction $^{12}C(^{16}O,\alpha)^{24}Mg_{g.s.}$ at $E(^{16}O)=63$ and 66 MeV in the range $\Theta_{c.m.}=8.5°$–$101.3°$ and are shown in Figs. 6(a) and 6(b), respectively.

The analyses of excitation functions and angular distribution data are discussed in the next section.

IV. ANALYSIS OF DATA

The excitation functions shown in Fig. 2 for the reaction $^{12}C(^{16}O, ^{8}Be)^{20}Ne$ and in Figs. 3, 4, and 5 for the reaction $^{12}C(^{16}O,\alpha)^{24}Mg$ leading to various excited states of ^{20}Ne and ^{24}Mg, respectively, cover the region of excitation 42–56 MeV in the compound nucleus ^{28}Si. All the excitation functions show prominent structures. The essential motivation in the present work is to identify structures in the excitation functions which are due to compound nuclear resonances as distinct from statistical fluctuations due to overlapping levels [16]. It is well established in the literature that the presence of cross correlations between different exit channels for the observed structures in the excitation functions is the significant evidence of intermediate resonance structures as opposed to statistical fluctuations [17,18]. Before presenting the details of this analysis we compare the measured cross sections with the expectations from the statistical model in the case of the reaction $^{12}C(^{16}O,\alpha)^{24}Mg$ leading to several discrete states.

A. Hauser-Feshbach statistical-model calculations

The statistical-model calculations are made based on the Hauser-Feshbach formalism [19], which reflects the average compound nucleus cross sections. In such a case the differential cross section is expressed as [20]

$$\frac{d\sigma_{\alpha\alpha'}}{d\Omega}=\sum_L \frac{\lambda^2}{4}\sum_J \frac{1}{(2I+1)(2i+1)}\frac{[\sum_{s,l}T_l(\alpha)]^J[\sum_{s',l'}T_{l'}(\alpha')]^J}{[\sum_{\alpha'',s'',l''}T_{l''}(\alpha'')]^J}Z(lJlJ,SL)Z(l'Jl'J,S'L)(-1)^{S-S'}P_L(\cos\theta)\ , \quad (1)$$

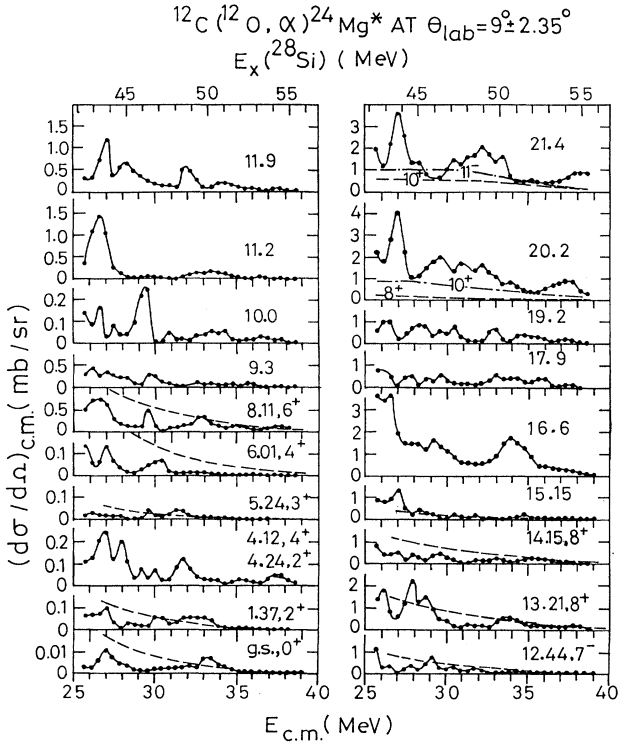

FIG. 4. Excitation functions for the reaction $^{12}C(^{16}O,\alpha)^{24}Mg$ at $\Theta_{lab}=9°$. Other details are the same as Fig. 3.

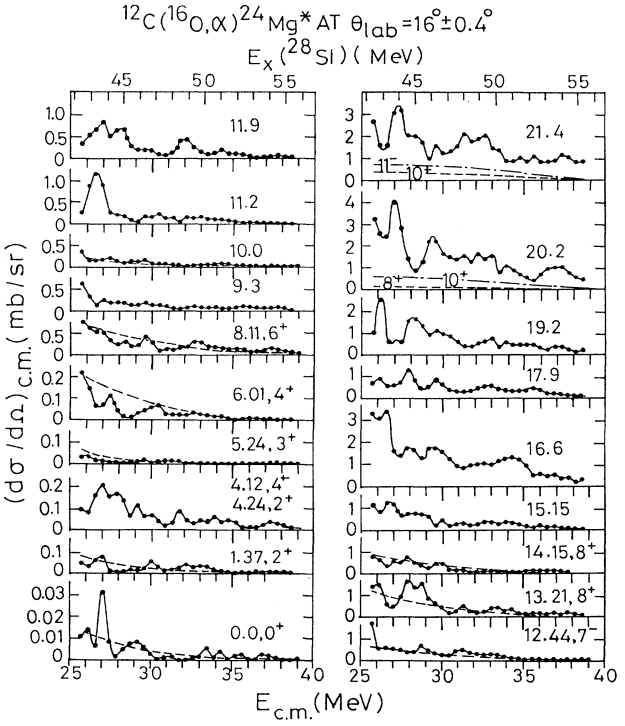

FIG. 5. Excitation functions for the reaction $^{12}C(^{16}O,\alpha)^{24}Mg$ at $\Theta_{lab}=16°$. Other details are the same as Fig. 3.

where α and α' specify the incident and the exit channels, respectively, and l the orbital angular momentum, S the channel spin, and I and i intrinsic angular momenta for the target and projectile. Primed symbols denote corresponding quantities in the exit channel. J denotes the compound nuclear angular momentum and T_l's are the transmission coefficients. The transmission coefficients T_l were computed with a computer program for optical-model calculations. The optical-model parameters for all the channels used and the level density parameters are the same as used in our analysis of the reaction $^{24}Mg(\alpha,^{12}C)^{16}O$ reported in Ref. [21]. A program HAFEST [21] was employed for the computation of these statistical-model calculations for the average compound nucleus cross sections. The calculated differential cross sections with Eq. (1) at different energies are shown for the reaction $^{12}C(^{16}O,\alpha)^{24}Mg$ at 6°, 9°, and 16° by dashed lines in Figs. 3, 4, and 5, respectively. These are shown

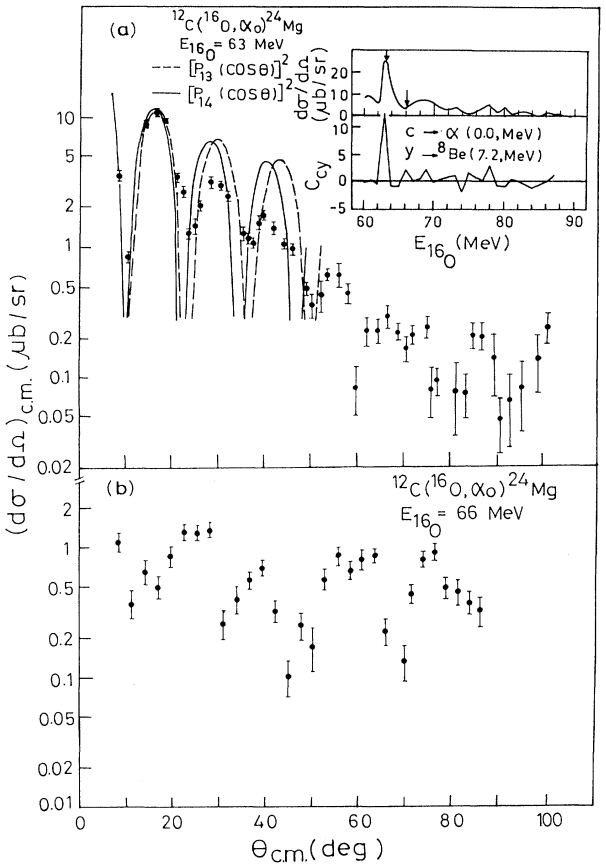

FIG. 6. (a) Angular distribution for the reaction $^{12}C(^{16}O,\alpha)^{24}Mg$ at "ON" resonance energy of $E(^{16}O)=63$ MeV. The data points are shown by closed circles with statistical error bars. The $[P_l(\cos\Theta)]^2$ are also shown. The inset shows the excitation function for this reaction indicating resonance at $E(^{16}O)=63$ MeV and cross-correlation function C_{cy} for correlation with the ^{8}Be channel leading to the 7.2 MeV state of ^{20}Ne. (b) Angular distribution for the same reaction at "OFF" resonance energy of $E(^{16}O)=66$ MeV.

for those excited states of ^{24}Mg which are found to show isolated alpha particle peaks in the spectra as judged from the peak widths. The spins of the excited states are taken from Ref. [22] for use in these calculations. The alpha particle peaks in the spectra corresponding to 20.2 and 21.4 MeV excitations in ^{24}Mg are also possibly single states as judged from the widths of these peaks. From the excitation functions for these states, deduced after subtracting the continuum below them and shown in Figs. 3–5, it is seen that these two states are excited with significantly large cross sections. The Hauser-Feshbach calculation for the expected cross section for the 20.2 MeV state is shown in Figs. 3–5 for spin assumptions of 8^+ and 10^+, respectively, and for the 21.4 MeV state for spin assumptions of 10^+ and 11^-. These are the highest possible spins which can be assumed for this excitation region in ^{24}Mg. It is for these spins of the residual states that the statistical-model predictions for the cross sections will be the highest and that is why these are shown in Figs. 3–5. As seen from these comparisons in the region from $E_{\text{c.m.}}=26$–33 MeV [bombarding energy range $E(^{16}\text{O})=61$–77 MeV] the measured cross sections are much larger than the statistical-model expectations. Whereas, for most of the lower-lying discrete states where statistical-model calculations are shown in Figs. 3–5, the average value of measured cross sections are in better agreement to the calculated values. Hence this may reflect more selective feeding of the states at 20.2 and 21.4 MeV in ^{24}Mg from these resonances in ^{28}Si due to nuclear structure reasons. In that case, these states of ^{24}Mg may not be of higher spin but states of lower spin and having strong structural overlap with the resonant states of ^{28}Si. This point is discussed further later.

Since the optical potential for the channel ^{8}Be+^{20}Ne is not reliably known, it is not considered suitable to make a similar comparison with statistical-model calculations in the case of reactions ^{12}C(^{16}O, ^{8}Be)^{20}Ne.

It is also relevant to point out that the step size in the center-of-mass system in the present work is 429 keV and the target thickness varies from 510 to 420 keV in the range of bombarding energies of 60–90 MeV. The coherence width of the fluctuations, which is equal to the average decay width Γ of the compound nuclear states, can be estimated from the empirical relation [16,18]

$$\Gamma = 14 \exp(-4.69\sqrt{A/E_x}) \text{ MeV} , \tag{2}$$

where A is the mass number and E_x is the excitation energy in MeV of the compound nucleus. This empirical estimate varies from 304 to 508 for $E_x=42$–56 MeV which is the region of excitation in ^{28}Si covered in the present work. Statistical fluctuation analysis of the data of the reaction ^{12}C(^{16}O,α)^{24}Mg and its inverse in different energy ranges exists in the literature [17,21,23] in which coherent widths have been obtained agreeing with the above empirical relation. In this context, the conditions of the present work are such that step size is about equal to the coherence width and hence are not suitable for deriving value of Γ from the data. However, in the present work, the simultaneous excitation function data leading to several discrete states in the reactions ^{12}C(^{16}O, ^{8}Be)^{20}Ne and ^{12}C(^{16}O,α)^{24}Mg enable cross channel correlation analyses which provide distinct evidence for intermediate resonance structures, which may be present in the midst of statistical fluctuations [18].

B. Cross channel correlations

The energy dependent cross-correlation function between channels i and j can be defined as [18,21,24]

$$C_{ij}=\frac{\left[\frac{d\sigma_i(E)}{\langle d\sigma_i(E)\rangle}-1\right]\left[\frac{d\sigma_j(E)}{\langle d\sigma_j(E)\rangle}-1\right]}{[R_i(0)R_j(0)]^{1/2}} , \tag{3}$$

where

$$R_i(0)=\left\langle \frac{d\sigma_i^2(E)}{\langle d\sigma_i(E)\rangle^2}-1\right\rangle_{\text{av}} , \tag{4}$$

where $\langle d\sigma_i(E)\rangle$ is a running average for the excitation function of channel i and $\langle\ \rangle_{\text{av}}$ means an average over the entire excitation function. When one considers N excitation functions the energy-dependent cross-correlation function can be defined as [18]

$$C(E)=\frac{2}{N(N-1)}\sum_{i>j=1}^{N} C_{ij}(E) . \tag{5}$$

In Fig. 7 the energy-dependent cross-correlation functions calculated with the above procedure are shown. The running average of 9 step size was used. Figure 7(a) shows the values of $C(E)$ calculated for all the 24 excitation functions measured, i.e., ($N=24$), 19 excitation functions for the reactions ^{12}C(^{16}O,α)^{24}Mg leading to different states of ^{24}Mg either resolved or unresolved and 5 excitation functions of ^{12}C(^{16}O,^{8}Be)^{20}Ne leading to states of ^{20}Ne. In the case of the reaction ^{12}C(^{16}O,α)^{24}Mg the excitation function measurements recorded at $\Theta_{\text{lab}}=6°$, 9°, and 16° (Figs. 3, 4, and 5, respectively) are all summed for each energy after multiplication with the $\sin\Theta_{\text{c.m.}}$ factor. These 19 summed excitation functions are taken for cross-correlation analysis. The maxima in values of $C(E)$ occur at energies $E(^{16}\text{O})=63$, 69, 72, 77, and 81 MeV. However, as a consequence of the cross-section averaging procedure the $C(E)$ functions produce maxima, associated to maxima as well as minima in excitation functions. To examine these cross correlations further some selected cross-correlation functions $C_{ij}(E)$ are shown in Figs. 7(b)–7(g). These are the cross correlation of alpha channels leading to a 20.2 and 21.4 MeV states in ^{24}Mg (where significantly large cross sections were observed as discussed earlier) with ^{8}Be channels leading to the ground state of ^{20}Ne as well as to states near 7.2 and 9.0 MeV. Denoting these alpha channels as a and b and ^{8}Be channels as x, y, and z, respectively, the energy-dependent cross channel correlation functions C_{bz}, C_{az}, C_{by}, C_{ay}, C_{bx}, and C_{ax} are shown in Figs. 7(b)–7(g), respectively. From these it is noticed that at $E(^{16}\text{O})=63$ MeV where the first maximum is seen in $C(E)$ [Fig. 7(a)] maxima are also observed in C_{bz}, C_{az}, C_{by}, C_{ay} [Figs. 7(b)–7(e)] and not in C_{bx}, C_{ax} [Figs. 7(f) and 7(g)]. Particularly, the cross-correlation coefficient is significantly large in C_{by}

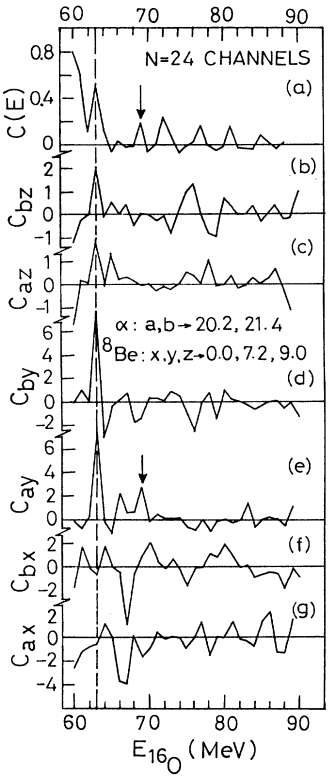

FIG. 7. Energy-dependent cross-correlation functions (a) $C(E)$ for $N=24$ channels which include 19 α channels and 5 ^{8}Be channels, (b)–(g) show cross-correlation functions between indicated alpha and ^{8}Be channels (see text). Significant cross correlations at $E(^{16}O)=63$ MeV are shown by vertical dashed line and at $E(^{16}O)=69$ MeV by arrows.

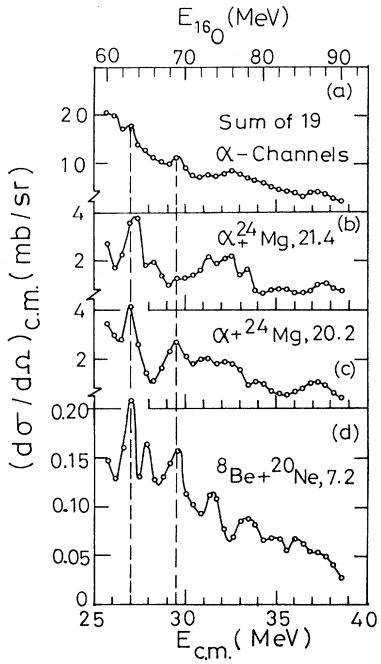

FIG. 8. Selected excitation functions: (a) Sum of 19 α channels in the reaction $^{12}C(^{16}O,\alpha)^{24}Mg^{*}$; (b) α channel leading to the 21.4 MeV state in ^{24}Mg; (c) α channel leading to the 20.2 MeV state in ^{24}Mg; (d) ^{8}Be channel in the reaction $^{12}C(^{16}O,^{8}Be)^{20}Ne$ leading to the 7.2 MeV state in ^{20}Ne. Cross correlated maxima are shown by vertical dashed lines at $E(^{16}O)=63$ and 69 MeV (see text).

and C_{ay} [Figs. 7(d) and 7(e)] at this energy showing significant cross correlation between ^{8}Be channels leading to states near 7.2 MeV in ^{20}Ne and alpha channels leading to a 20.2 and 2.14 MeV states in ^{24}Mg. The cross correlation is also present between ^{8}Be channels leading to states near 9.0 MeV and alpha channels leading to 20.2 and 21.4 MeV states of ^{24}Mg [Figs. 7(b) and 7(c)] at this energy. It is significant to note that this cross correlation is absent to ground state of ^{20}Ne [Figs. 7(f) and 7(g)].

At $E(^{16}O)=69$ MeV where $C(E)$ shows maximum [Fig. 7(a)] C_{ay} [Fig. 7(e)] also shows maximum indicating that at this energy cross correlation is present between ^{8}Be channels leading to states near 7.2 MeV in ^{20}Ne and alpha channels leading to a 20.2 MeV state of ^{24}Mg.

Out of these maxima in $C(E)$ and $C_{ij}(E)$, to identify those which are associated with significant maxima in excitation functions selected excitation functions are shown in Fig. 8. Figure 8(a) shows the summed excitation function of 19 alpha channels (summed over all angles data) of the reaction $^{12}C(^{16}O,\alpha)^{24}Mg$ while Figs. 8(b) and 8(c) show the excitation functions for the reaction $^{12}C(^{16}O,\alpha)^{24}Mg$ leading to 21.4 and 20.2 MeV states of ^{24}Mg, respectively. Figure 8(d) shows the excitation functions for the reaction $^{12}C(^{16}O,^{8}Be)^{20}Ne$ leading to peak corresponding states near 7.2 MeV. At $E(^{16}O)=63$ MeV where $C(E)$ shows maximum in Fig. 7(a), the significant maxima are observed in Figs. 8(a)–8(d) while at $E(^{16}O)=69$ MeV where $C(E)$ shows maximum in Fig. 7(a) we observe maxima in Figs. 8(a), 8(c), and 8(d). Therefore, at $E(^{16}O)=63$ MeV resonance structure is observed with cross-channel correlations observed in ^{8}Be channel leading to 7.2 MeV state peak as well as in alpha channels leading to 20.2 and 21.4 MeV states in ^{24}Mg. In a summed excitation function summed over all 19 alpha channels, the maximum occurring at this energy provides further evidence of the resonance structure at this energy since any statistical fluctuation would be smeared out when so many channels are summed. Similarly at $E(^{16}O)=69$ MeV resonance structure can be confirmed with cross correlation present between ^{8}Be channels leading to states near 7.2 MeV and alpha channels leading to a 20.2 MeV state in ^{24}Mg. This resonance structure at $E(^{16}O)=69$ MeV is also significantly present in the summed excitation function, summed over 19 alpha channels [Fig. 8(a)].

C. Angular distributions in $^{12}C(^{16}O,\alpha)^{24}Mg$

At $E(^{16}O)=63$ MeV cross correlation is observed among several channels, particularly between ^{8}Be channels leading to a 7.2 MeV state of ^{20}Ne and alpha channels leading to 20.2 and 21.4 MeV states of ^{24}Mg. This resonance structure at $E(^{16}O)=63$ MeV also shows a

weak peak in the excitation function for the alpha channel leading to ground state of ^{24}Mg in the reaction ^{12}C(^{16}O,α)^{24}Mg as shown in the inset of Fig. 6(a) where the excitation function summed over all the angles is plotted. The energy-dependent cross-correlation function C_{cy} between this channel (denoted by c) and the ^{8}Be channel leading to a 7.2 MeV state of ^{20}Ne (denoted by y), shown in the inset of Fig. 6(a), clearly shows a maximum at $E(^{16}\text{O})=63$ MeV resonance. Hence, the angular distributions of the reaction ^{12}C(^{16}O,α)^{24}Mg$_{\text{g.s.}}$ was measured for determination of the spin of the $E(^{16}\text{O})=63$ MeV resonance. In this reaction leading to ground state of ^{24}Mg, since all the particles involved are spinless any angular distribution that is dominated by a single partial wave l will obey the squared Legendre-polynomial expression as follows [2]

$$\frac{d\sigma}{d\Omega} \propto [P_l(\cos\Theta)]^2 . \tag{6}$$

The angular distribution data shown in Fig. 6(a) were recorded at $E(^{16}\text{O})=63$ MeV. The angular distribution shows prominent oscillatory structure. Figure 6(b) shows the angular distribution data measured at $E(^{16}\text{O})=66$ MeV which is "OFF" resonance energy. At this energy maximum cross section is around 1 μb/sr. At the "ON" resonance energy of $E(^{16}\text{O})=63$ MeV, the angular distribution data [Fig. 6(a)], in the forward peaks where the cross section is well above the 1 μb/sr level, are compared with calculated curve for $[P_{14}(\cos\Theta)]^2$ and $[P_{13}(\cos\Theta)]^2$ normalized at the first peak. The peak positions agree with the data for $[P_{14}(\cos\Theta)]^2$ while for $[P_{13}(\cos\Theta)]^2$, the agreement is slightly worse.

The intensities beyond the first peak keep falling due to some interferences. Beyond about $\Theta_{\text{c.m.}}=50°$ cross sections are very low similar to the "OFF" resonance data in Fig. 6(b). From the positions of the peaks in the angular distribution data we infer the spin of the $E(^{16}\text{O})=63$ MeV resonance to be $J=l=14$.

V. RESULTS AND DISCUSSIONS

From the analysis of data the following points emerge.

At energies corresponding to $E(^{16}\text{O})=63$ and 69 MeV resonance structures are present in the excitation functions. The first resonance at bombarding energy at $E(^{16}\text{O})=63$ MeV corresponds to $E_{\text{c.m.}}=26.9$ MeV (after allowing for half of the target thickness). This resonance corresponding to excitation energy of 43.7 MeV in ^{28}Si decays through the ^{8}Be channel to the 7.2 and 9.0 MeV states in ^{20}Ne and not to the ground state or to the ground-state band members. Experimental investigations of Middleton, Garrett, and Fortune [25] and Hindi *et al.* [26] have provided evidence suggesting a 7.2 MeV state of ^{20}Ne to be a 8-particle–4-hole state. They also conclude 7.20 MeV 0^+, 7.83 MeV 2^+, and 9.04 MeV 4^+ states of ^{20}Ne to be the first three members of the rotational band built on the $8p$-$4h$ state.

This resonance decays also by alpha channels to the 20.2 and 21.4 MeV states of ^{24}Mg with cross sections significantly larger than expected from statistical-model calculations. The width of the resonance is about 600 keV and the spin parity can be assigned as 14^+ from the present data.

The second resonance at bombarding energy $E(^{16}\text{O})=69$ MeV corresponding to $E_{\text{c.m.}}=29.5$ MeV (after allowing for half the target thickness) decays in the ^{8}Be channel to the 7.2 MeV 8-particle–4-hole state of ^{20}Ne. It also decays in the alpha channel to the 20.2 MeV state of ^{24}Mg with a cross section much larger than expected from statistical-model calculations. The width of this resonance at excitation energy of 46.2 MeV in ^{28}Si is estimated to be about 900 keV from the present data. Bechara *et al.* [24] have studied the excitation functions for the reaction ^{12}C(^{16}O,α)^{24}Mg* in the energy range partially overlapping with that studied in the present work. They have identified nonstatistical structures at $E_{\text{c.m.}}=29.5$, 32.2, 35.0, and 37.3 MeV. The resonance structure at $E(^{16}\text{O})=69$ MeV ($E_{\text{c.m.}}=29.5$ MeV) identified in the present work agrees with the first structure referred in their work. Corresponding to $E_{\text{c.m.}}=32.2$ and 37.3 MeV noted in their work, peaks are observed in our work in the excitation function shown [Fig. 8(a)] for the sum of 19 alpha channels.

Figure 9 presents a plot of $E_{\text{c.m.}}$ vs $J(J+1)$ for the resonances in the system ^{16}O+^{12}C observed in the literature with spins measured. These resonances have been identified through elastic, inelastic scattering channels and ^{8}Be and alpha decay channels [27–37]. The $E_{\text{c.m.}}=26.9$ MeV resonance identified in the present work with J^π assignment of 14^+ is also shown in the

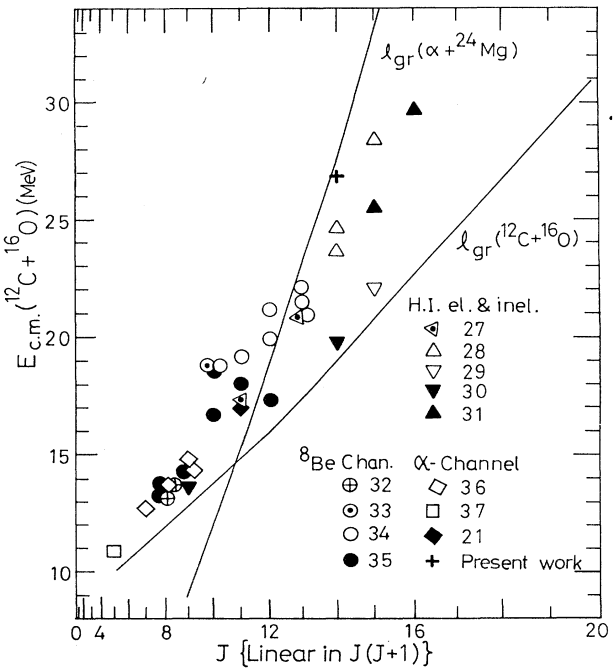

FIG. 9. Plot of E vs $J(J+1)$ showing observed resonances in the system ^{12}C+^{16}O from the literature. The resonance at $E_{\text{c.m.}}=26.9$ MeV with $J^\pi=14^+$ identified in the present work is also shown. The curves show the calculated l_{gr} values for $\alpha+^{24}$Mg and ^{12}C+^{16}O channels.

figure. The second resonance identified at $E_{c.m.}=29.5$ MeV in the present work is not shown in the figure since the spin is not known. In the figure we have also shown curves corresponding to grazing l values for $^{12}C+^{16}O$ and $\alpha+^{24}Mg$ channels calculated with optical-model potentials [21] mentioned earlier for statistical-model calculations. The grazing l values l_{gr} is determined corresponding to transmission coefficient $T_l=0.5$. The reported J values are from one to three units less than the l_{gr} for $^{12}C+^{16}O$ up to $E_{c.m.}=25$ MeV and more than this for higher energies. The resonance reported in the present work at $E_{c.m.}=26.9$ MeV with $J=14$ is four units less than the $l_{gr}=18$ for the $^{16}O+^{12}C$ incident channel, but it agrees with l_{gr} value for the exit channel $\alpha+^{24}Mg$. This is an indication that the intermediate resonance structures are not due to entrance channel effects associated with the grazing l values.

The two resonances identified in the present work show clear evidence for decay in ^{8}Be and alpha channels to selected states in ^{20}Ne and ^{24}Mg. We infer from these selective particle decays the special characteristics of the compound nuclear states represented by the resonances.

Before going into the details of this interpretation it is necessary to point out certain features regarding the nature of the states in ^{20}Ne fed by ^{8}Be decay channel as identified in the present work.

Since the overall resolution of the peaks in the ^{8}Be spectrum is about 550 keV the peak corresponding to 7.2 MeV excitation in ^{20}Ne can also include states in ^{20}Ne at 6.72 MeV 0^+, 7.43 MeV 2^+, and 7.17 MeV 3^-. However, these states in ^{20}Ne have been identified as having $^{16}O+\alpha$ character by experimental [25,26] and theoretical [38] studies while 7.2 MeV 0^+ and 7.83 MeV 2^+ have been well established as the members of the band with $8p$-$4h$ character [25,26]. Since the resonances at $E_{c.m.}=26.9$ and 29.5 MeV in the present work do not feed the ground-state band of ^{20}Ne which have $^{16}O+\alpha$ character it can be taken that any contribution in the ^{8}Be spectrum to the 7.2 MeV state peak from the 6.72, 7.43, and 7.17 MeV states of ^{20}Ne is negligible. Hence the two resonances decay to the 7.2 MeV state of $8p$-$4h$ character and not to the states of $^{16}O+\alpha$ character. Even through the energy available for ^{8}Be decay is more by about 7 MeV to the ground state than to the 7.2 MeV quartet state and both these states have $J^{\pi}=0^+$, the resonances decay dominantly to the quartet state. Purely from penetrability considerations opposite will be the case. Hence it can be deduced that there is a nuclear structural reason for this mode of decay. These decay modes of the two resonances are shown by arrows in the energy-level diagram in Fig. 10.

Leander and Larsson [39] have shown by calculations of potential-energy surfaces based on the Nilsson-Strutinsky procedure, that the triaxial secondary minimum of ^{20}Ne corresponds to an 8-particle–4-hole state relative to ^{16}O and suggest that the $E_x=7.2$ MeV state is possibly such a state. As stated earlier, Middleton, Garrett, and Fortune [25] and Hindi *et al.* [26] suggest based on their experimental investigations that the state at $E_x=7.2$ MeV be an $8p$-$4h$ state and propose the first three members of the rotational band to be $E_x=7.20$ MeV 0^+, 7.83 MeV 2^+, and 9.04 MeV 4^+. It is also expected from the calculations of Leander and Larsson [39] that the configuration of such a state would be a (2-proton,2-neutron)$^{-1}$ structure in a $0p$ shell and a $(2p,2n)^2$ structure in a $(0d,1s)$ shell ([220] in the notation of Arima, Gillet, and Ginocchio [40]), with a large deformation. The deformation parameters of this configuration corresponding to the triaxial minimum is predicted by calculations of Leander and Larsson [39] to be $\epsilon=1.17$, $\gamma=50°$ with an oscillator frequency ratio, $w_x:w_y:w_z=8:3:2$. The $(8p$-$4h)$ states in ^{20}Ne may also include [211] configurations. Leander and Larsson [39] calculations of potential-energy surfaces for ^{28}Si also predict configurations of $16p$-$4h$, with $(2p,2n)^{-1}$ in the $0p$ shell, $(2p,2n)^3$ in the $(0d,1s)$ shell, and $(2p,2n)^1$ in the $(0f,1p)$ shell (i.e.) [231] in the notation of Arima, Gillet, and Ginocchio [40] to be at the secondary minimum with deformation parameter of $\epsilon=1.35$ and $\gamma\approx 60°$. This corresponds to a promotion of the $(2p,2n)$ quartet from the $0p$ shell to the $(0f,1p)$ shell with respect to the ground state of ^{28}Si. Such configurations are possible above about 17

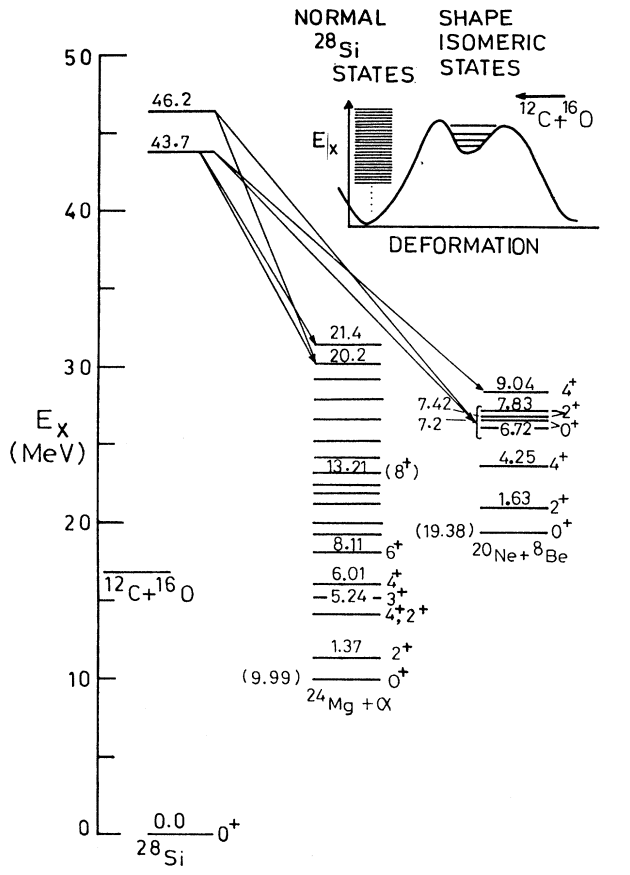

FIG. 10. Energy-level diagram showing the two resonances in the system $^{12}C+^{16}O$ identified in the present work. The strong correlated decay of the resonances in the α and ^{8}Be channels are shown by arrows. The energy levels in ^{24}Mg and ^{20}Ne shown in the figure are those for decay to which the excitation functions have been measured in the present work.

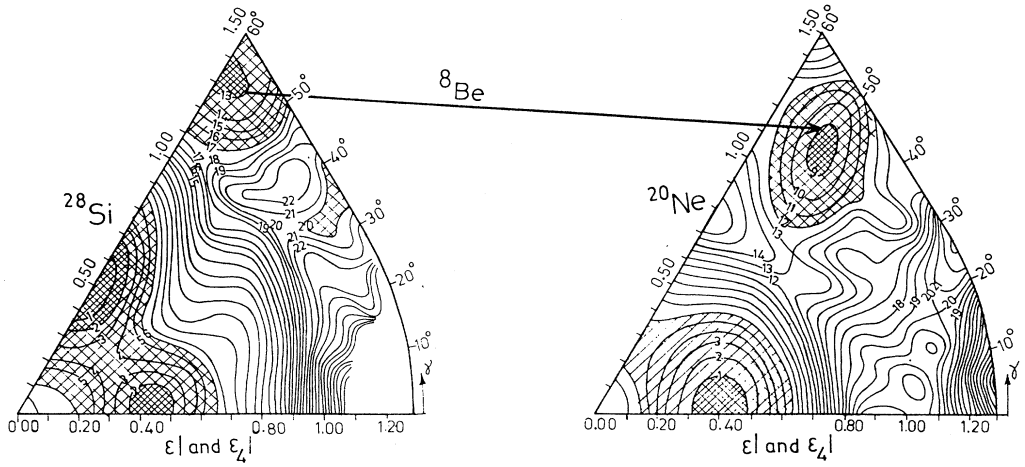

FIG. 11. Potential-energy surfaces for ^{28}Si and ^{20}Ne from the deformed shell-model calculations by Leander and Larsson (Ref. [39]). The thick arrow connecting the shape isomeric configurations of ^{28}Si and ^{20}Ne by the ^{8}Be decay mode is based on the observations in the present work. (See text.)

MeV excitation in ^{28}Si according to the calculation of Arima, Gillet, and Ginnochio [40].

We interpret our observation of decay of the resonances in the ^{16}O+^{12}C system at E_x=43.7 and 46.2 MeV in ^{28}Si to the quartet states of ^{20}Ne near 7.2 MeV in preference over the ground-state band members of ^{20}Ne to be the evidence for the resonances to be the higher rotational member states in ^{28}Si with intrinsic configurations at the superdeformed secondary minimum discussed above as expected in the Leander and Larsson [39] calculations. In other words, the selective ^{8}Be decay of the resonances are the transitions connecting the related configurations in ^{28}Si and ^{20}Ne. This is shown schematically in Fig. 11 where the potential-energy plot in terms of deformation parameters of ϵ and γ as calculated by Leander and Larsson for ^{28}Si and ^{20}Ne are shown with the arrow showing the transition connecting the related configurations as inferred from the present work.

In the work of Voit, Ischeriko, and Siller [41] the near Coulomb barrier ^{12}C+^{12}C resonance at 20.25 MeV excitation in ^{24}Mg and nearby ones are found to decay preferentially to quartet state near 7.2 MeV in ^{20}Ne. Further Fulton *et al.* [42] in a high-resolution measurement of the breakup reaction ^{12}C(^{24}Mg,^{12}C^{12}C)^{12}C find evidence for superdeformed shape isomeric nature of states as expected from Nilsson-Strutinsky calculations at an excitation region of 20–26 MeV in ^{24}Mg. In this study the states in the range 20–22 MeV are assigned $J^{\pi}=4^{+}$ and it is conjectured that these superdeformed shape isomeric states are ^{12}C+^{12}C resonance states.

Based on these observations of Voit, Ischeriko, and Siller [41] and Fulton *et al.* [42] we conjecture that the strong transitions of alpha decay of the two resonances identified in the present work at $E_{\text{c.m.}}$=26.9 and 29.5 MeV to the states at 20.2 and 21.4 MeV in ^{24}Mg may also be due to the fact that these states in ^{24}Mg have related configurations to the resonance states in ^{28}Si which decay preferentially to superdeformed 8-particle–4-hole states of ^{20}Ne. According to potential-energy calculations of Leander and Larsson [39] in the case of ^{24}Mg the superdeformed states in second minimum correspond to 12-particle–4-hole states with deformation parameters of $\epsilon=1.26$ and $\gamma=42°$ with oscillator frequency ratio $w_x:w_y:w_z=5:2:1$. In this context it is also relevant to note that Ledoux *et al.* [10] in their study of the ^{12}C(^{12}C,α)^{20}Ne reaction find resonances in the system ^{12}C+^{12}C showing enhanced decays to excited rotational bands in ^{20}Ne based on 8-particle–4-hole states. Based on these they interpret the resonances in ^{12}C+^{12}C system to be leading to superdeformed states of ^{24}Mg mentioned above which have configurations [221] in the notation of Arima, Gillet, and Ginocchio [40].

In summary, in the present work we have presented evidence for the identification of highly deformed structures in ^{28}Si formed as resonances in the system ^{16}O+^{12}C by observation of their preferential ^{8}Be decay to superdeformed quartet states in ^{20}Ne. In addition, strong alpha decays from these resonances to the 20–22 MeV excitation region of ^{24}Mg lends support to correlated superdeformed structures in ^{28}Si, ^{24}Mg, and ^{20}Ne as expected from deformed shell-model calculations.

ACKNOWLEDGMENTS

We acknowledge the cooperation of the operation staff in the smooth running of the Pelletron accelerator and our thanks are also due to H. H. Oza for assistance in various stages of the experiment.

[1] D. A. Bromley, in *Resonances in Heavy Ion Reactions,* Vol. 156 of *Lecture Notes in Physics,* edited by K. E. Eberhard (Springer, Berlin, 1982), p. 3.
[2] N. Cindro, Riv. Nuovo Cimento **4**, 1 (1981).
[3] H. J. Fink, W. Scheid, and W. Greiner, Nucl. Phys. **A188**, 259 (1972).
[4] W. Scheid, W. Greiner, and R. Lemmer, Phys. Rev. Lett. **25**, 176 (1970).
[5] B. Imanishi, Nucl. Phys. **A125**, 33 (1969).
[6] H. Chandra and U. Mosel, Nucl. Phys. **A298**, 151 (1978).
[7] I. Ragnarsson, S. Aberg, and R. K. Sheline, Phys. Scr. **24**, 215 (1981).
[8] A. S. Umar and M. R. Strayer, Phys. Lett. B **171**, 353 (1986).
[9] R. R. Betts, Comments Nucl. Part. Phys. **13**, 61 (1984), and references quoted therein.
[10] R. J. Ledoux, C. E. Ordonez, M. J. Bechara, H. A. Al-Jumair, G. Larelle, and E. R. Cosman, Phys. Rev. C **30**, 866 (1984).
[11] B. K. Dichter, P. D. Parker, S. J. Sanders, R. R. Betts, and S. Saini, Phys. Rev. C **35**, 1304 (1987).
[12] M. A. Eswaran, Suresh Kumar, E. T. Mirgule, D. R. Chakrabarty, V. M. Datar, U. K. Pal, and N. L. Ragoowansi, in *Proceedings of the International Conference on Nucleus-Nucleus Collisions IV,* Kanazawa, Japan (1991). [Nucl. Phys. Symp. (DAE), Bombay **34B**, 125 (1991)].
[13] G. J. Wozniak, N. A. Jelley, and Joseph Cerny, Nucl. Instrum. Methods **120**, 29 (1974).
[14] Suresh Kumar, M. A. Eswaran, and E. T. Mirgule, Nucl. Phys. Symp. (DAE) Bombay **34B**, 427 (1991).
[15] G. J. Wozniak, H. L. Harney, K. H. Wilcox, and J. Cerny Phys. Rev. Lett. **28**, 1278 (1972).
[16] D. M. Brink and R. O. Stephen, Phys. Lett. **5**, 77 (1963); T. E. O. Ericson and T. Mayer-kuckuk, Annu. Rev. Nucl. Sci. **16**, 183 (1966).
[17] M. L. Halbert, F. E. Durham, and A. Van der Woude, Phys. Rev. **162**, 899 (1967).
[18] L. C. Dennis, S. T. Thorton, and K. R. Cordell, Phys. Rev. C **19**, 777 (1979); R. L. Park, S. T. Thorton, K. R. Cordell, and C. A. Wiedner, *ibid.* **25**, 313 (1982).
[19] W. Hauser and H. Feshbach, Phys. Rev. **87**, 366 (1952).
[20] R. G. Skokstad, in *Treatise on Heavy-Ion Science,* edited by D. A. Bromley (Plenum, New York, 1985), Vol. 3, p. 83.
[21] M. A. Eswaran, Suresh Kumar, E. T. Mirgule, and N. L. Ragoowansi, Phys. Rev. C **39**, 1856 (1989).
[22] P. M. End and Van der Leun, Nucl. Phys. **A521**, 1 (1991).
[23] R. Singh, K. A. Eberhard, and R. G. Stokstad, Phys. Rev. C **22**, 1971 (1980).
[24] M. J. Bechara, A. J. Lazzarini, R. J. Ledoux, and E. R. Cosman, Phys. Rev. C **27**, 1540 (1983).
[25] R. Middleton, J. D. Garrett, and H. T. Fortune, Phys. Rev. Lett. **27**, 950 (1971).
[26] M. M. Hindi, J. H. Thomas, D. C. Radford, and P. D. Parkar, Phys. Lett. **99B**, 33 (1981); Phys. Rev. C **27**, 2902 (1983).
[27] P. Charles, F. Auger, I. Badawy, B. Berthier, M. Dost, J. Gastebois, B. Fernandez, S. M. Lee, and E. Plagnol, Phys. Lett. **62B**, 289 (1976).
[28] K. Katori, K. Furuno, and T. Ooi, Phys. Rev. Lett. **40**, 1489 (1978); K. Katori, K. Furono, T. Ooi, and S. Hanashima, Phys. Rev. C **21**, 1387 (1980).
[29] D. Shapira, R. M. De Vries, M. R. Clover, R. N. Boyd, and R. N. Cherry, Jr., Phys. Rev. Lett. **40**, 371 (1978).
[30] R. E. Malmin, J. W. Harris, and P. Paul, Phys. Rev. C **18**, 163 (1978).
[31] C. M. Jachcinski, P. Braun-Munzinger, G. M. Berkowitz, R. H. Freifelder, M. Gai, T. R. Renner, and C. D. Uhlhorn, Phys. Rev. C **22**, 101 (1980).
[32] F. P. Brady, D. A. Viggars, T. W. Conlon, and D. J. Parkar, Phys. Rev. Lett. **39**, 870 (1977); D. A. Viggars, T. W. Conlon, F. P. Brady, and I. Naqib, Phys. Rev. C **19**, 2186 (1979).
[33] K. A. Eberhard, H. Bohn, and K. G. Bernhardt, Phys. Rev. Lett. **42**, 432 (1979).
[34] D. R. James and N. R. Fletcher, Phys. Rev. C **20**, 560 (1979).
[35] J. R. Hurd, N. R. Fletcher, A. D. Frawley, and J. F. Mateja, Phys. Rev. C **22**, 528 (1980).
[36] F. Soga, J. Schimizu, H. Kamitsubo, N. Takahashi, K. Takimoto, R. Wada, T. Fujisawa, and T. Wada, Phys. Rev. C **18**, 2457 (1978).
[37] N. Cindro, G. Vourvopoulos, X. Aslanoglou, G. Andritsopoulos, P. Assimakopoulos, and B. Bakoyorgos, J. Phys. G **5**, 309 (1979).
[38] Y. Fujiwara, Prog. Theor. Phys. **62**, 122 (1979); **62**, 138 (1979); Y. Fujiwara, H. Horiuchi, and R. Tamagaki, *ibid.* **61**, 1629 (1979); T. Tomoka and A. Arima, Nucl. Phys. **A303**, 217 (1978).
[39] G. Leander and J. E. Larsson, Nucl. Phys. **239A**, 93 (1975).
[40] A. Arima, V. Gillet, and J. Ginocchio, Phys. Rev. Lett. **25**, 1043 (1970).
[41] H. Voit, G. Ischeriko, and F. Siller, Phys. Rev. Lett. **30**, 564 (1973).
[42] B. R. Fulton, S. J. Bennett, M. Freer, J. T. Murgatroyd, G. J. Gzapong, N. S. Jarvis, C. D. Jones, D. L. Watson, J. D. Brown, W. D. M. Rae, A. E. Smith, and J. S. Lilley, Phys. Lett. B **267**, 325 (1991).